RSC Advances

ROYAL SOCIETY OF CHEMISTRY

www.rsc.org/advances

Targeted photosensitizer nanoconjugates based on human serum albumin selectively kill tumor cells upon photo-irradiation

Cheng-Yi Tang [a,b,1], Yong-hui Liao [a,1], Xiao-Ming Wang [a,b], Gui-Hua Lu [a,b] and Yong-Hua Yang [a,b,*]

Affiliations:

[a]State Key Laboratory of Pharmaceutical Biotechnology, NJU-NJFU Joint Institute of Plant Molecular Biology, School of Life Sciences, Nanjing University, Nanjing 210093, China.

[b]Co-Innovation Center for Sustainable Forestry in Southern China, Nanjing Forestry University, Nanjing 210037, China

[1]These authors contributed equally.

*Corresponding author. Tel/fax: +86-25-89686305

E-mail address: yangyh@nju.edu.cn

Abstract

A photosensitizer (Chlorin e6, Ce6) nanoconjugate based on human serum albumin (HSA) was designed and prepared for tumor cell targeted photodynamic therapy. The resulting nanoconjugates consisted of multiple cyclic Arg-Gly-Asp-D-Tyr-Cys peptides (cRGD) and about 5.4 Ce6 on each HSA molecule (RGD-HSA-Ce6). RGD-HSA-Ce6 exhibited small size with a mean diameter of 31.1 nm and negative charge with -15.9mV. Due to the incorporation of targeting moiety, RGD-HSA-Ce6 could be specifically recognized by αvβ3 integrin overexpressed tumor cells, as well as internalized into late endosomes and lysosomes efficiently. In addition, RGD-HSA-Ce6 exhibited low dark toxicity in both tumor and normal cell lines. Upon photo-irradiation, RGD-HSA-Ce6 exhibited high phototoxicity against αvβ3 integrin overexpressed A375 melanoma cells, indicating the considerable potential for effective photodynamic therapy. Combined with the low phototoxicity to normal fibroblast 3T3 cells, RGD-HSA-Ce6 developed in this study may provide an effective tool for targeted photodynamic therapy to tumor cells.

1. Introduction

Photodynamic therapy (PDT) employs three essential elements to induce cell death: photosensitizer (PS), light of particular wavelength, and oxygen.[1] In general, the activated PS reacts directly with oxygen to form cytotoxic singlet oxygen that damages lipids, proteins and other cellular components.[2, 3] As singlet oxygen is short-lived and has very short diffusion distance,[4, 5] its cytotoxicity depends largely on the localization of photosensitizer upon photo-irradiation.[6] However, the clinical application of PDT is limited due to poor solubility and low tumor selectivity of PSs.[7-10] Therefore, many researchers made efforts to render PSs more hydrophilic or tumor-targeting through chemical modifications or nanosized delivery systems.[11-13]

Human serum albumin is abundant in plasma and it keeps quite stable in the pH range 4-9.[14-17] These properties, as well as its excellent biocompatibility make HSA an ideal carrier for drug/photosensitizer delivery.[18, 19] For instance, Jeong *et al.* incorporated Ce6, a photosensitizer, into albumin nanoparticles (Ce6-HSA-NPs) for PDT.[20] The formulation of nanoparticles increased the solubility of Ce6 in aqueous solution. However, Ce6-HSA-NPs did not exhibit improved singlet oxygen generation and PDT activity in vitro when compared with free Ce6, which was likely due to the lack of tumor-targeting of Ce6-HAS-NPs. To further develop a more effective PDT, introducing tumor-targeting moiety into photosensitizer delivery systems is really necessary.

Integrin αvβ3 has crucial roles in tumor angiogenesis and metastasis, and is overexpressed on tumor new-blood vessels and some tumor cells, which makes αvβ3 integrin a suitable target for tumor therapy.[21-23] Arg-Gly-Asp (RGD) peptide could selectively bind αvβ3 integrin for effectively tumor-targeting delivery.[24-27] For instance, RGD peptide conjugated to NIR fluorescent dye could specifically target integrin both in vitro and in vivo.[28] In addition, RGD grafted polymeric nanoparticles showed higher affinity to αvβ3 integrin

overexpressed tumor cell lines than non-targeted nanocarriers.[29-31]

In this study, we modified albumin with multiple targeting moiety cRGD which can selectively bind to αvβ3 integrin overexpressed on tumor cells. Then photosensitizer Ce6 molecules were covalently conjugated to the cRGD functionalized HSA to form RGD-HSA-Ce6 nanoconjugates. The obtained RGD-HSA-Ce6 was characterized in terms of size, zeta potential, and singlet oxygen generation. The cellular uptake and trafficking of RGD-HSA-Ce6 were also evaluated. In vitro studies demonstrated that RGD-HSA-Ce6 preferentially internalized into αvβ3 integrin overexpressed A375 tumor cells and localized in the late endosomes and lysosomes. Finally, RGD-HSA-Ce6 exhibited significantly higher laser-triggered phototoxicity to A375 cells compared to fibroblast 3T3 cells with lower αvβ3 integrin expression. These results indicated that RGD-HSA-Ce6 was an attractive photosensitizer delivery system for targeted PDT.

2. Materials and methods:

2.1 Materials

Human serum albumin (≥96%, pharmaceutical grade) was obtained from CSL Behring GmbH (Marburg, Germany). cRGD was obtained from GL Biochem Ltd (Shanghai, China). EDC, Sulfo-NHS and Ce6 were purchased from Sigma-Aldrich Co., LLC (USA). Mal-PEG_{5K}-NHS was purchased yarebio Ltd (Shanghai, China). Sephadex LH-20 was purchased from GE Healthcare (PA, USA). Cell counting kit-8 (CCK-8) was supplied by Dojindo Laboratories (Kumamoto, Japan). Singlet oxygen sensor green (SOSG) was obtained from Life Technologies. CellLight® Early Endosomes-GFP, Late Endosome-GFP, Lysosome-GFP and Mitochondria-GFP were obtained from Life Technologies (Rockford, USA).

2.2 Preparation and characterization of RGD-HSA-Ce6

Human serum albumin and Mal-PEG_{5K}-NHS were mixed at 1:15 molar ratio in PBS (pH 7.4) at room temperature for 1h. Then cRGD was added to conjugate with the maleimide group of PEG for another 1h at the molar ratio of cRGD to HSA as 20:1. Ce6 was dissolved in DMSO, and activated by incubating 5 molar equivalents of EDC and Sulfo-NHS overnight. After that, activated Ce6 was added into the above RGD-HSA conjugates with an 8:1 molar ratio of Ce6 to HSA and the solution were gently stirred for 12h in dark at room temperature. The conjugated RGD-HSA-Ce6 was purified with column chromatography. For the purification, the crude products were chromatographed using a column filled with Sephadex LH-20 as the stationary phase and mixed methanol/water (v/v=1:4) solvent served as the mobile phase. The fraction of RGD-HSA-Ce6 was easily eluted from the column because there was not obvious binding between RGD-HSA-Ce6 and LH-20 medium. Due to the hydrophobic binding between free Ce6 and LH-20 medium, methanol should be used to elute the bound free Ce6. Then the obtained

RGD-HSA-Ce6 was concentrated under speed vacuum and the Ce6 content of RGD-HSA-Ce6 was measured at the 403nm absorption peak. The concentration of albumin of RGD-HSA-Ce6 conjugates was detected by BCA assay.

The fluorescence of free Ce6 and RGD-HSA-Ce6 (10μM of Ce6) was detected by Fluorescence Spectroscopy (RF-5301, Shimadzu Scientific Instruments). Ce6 and RGD-HSA-Ce6 were distributed in PBS or PBS/Methanol (v/v=1/1) mixed solvent, respectively.

Fluoraldehyde™ o-Phthaldialdehyde Crystals (OPA, Thermo Scientific) was used to detect the primary amine of HSA, RGD-PEG-HSA and RGD-HSA-Ce6. OPA could react with primary amine of protein to yield fluorescent derivatives (ex/em = 340nm/455nm). In each group, 200μl OPA reagent was mixed with 20 μl sample of each group containing 5μM albumin. Then fluorescence was detected by Tecan microplate reader (Switzerland).

To compare the singlet oxygen generation of RGD-HSA-Ce6 and free Ce6 (5μM of Ce6), the singlet oxygen sensor green (SOSG) was introduced at a concentration of 2.5μM. Singlet oxygen was produced by photo-irradiation with a 670nm laser with the intensity of 5mW/cm^2. After photo-irradiation, SOSG fluorescence was read at an excitation and emission of 488 and 525 nm, respectively, to determine the singlet oxygen generation of RGD-HSA-Ce6 and free Ce6. The hydrodynamic size and zeta potential of RGD-HSA-Ce6 were measured by Zetasizer Nano (Malvern Instruments, Malvern, UK). The morphology of RGD-HSA-Ce6 was observed using a Transmission Electron Microscope (TEM, JEM-200CX, JEOL).

2.3 Cell culture and intracellular uptake

To test the targeting effect of RGD-HSA-Ce6, A375 cells (human melanoma) with overexpressed αvβ3 integrin on the cellular membrane were chosen as integrin-positive tumor cell line, while 3T3 cells (mouse fibroblasts)

with low αvβ3 integrin expression were used as the negative control. A375 and 3T3 cells were both cultured in DMEM medium +10% FBS and 1% penicillin/streptomycin at 37°C and 5% CO_2. After attachment, A375 cells and 3T3 cells were treated with 200nM of free Ce6 or RGD-HSA-Ce6. Free cRGD was used for blocking αvβ3 integrin. 12h later, cells were rinsed by PBS, then trypsinzed, and resuspended in fresh culture medium. Flow cytometry was performed to detect the Ce6 fluorescence (Excitation: 405nm, Emission: 670/20nm).

Confocal microscopy was also used to detect the cellular uptake of free Ce6 and RGD-HSA-Ce6. A375 cells were seeded in glass-bottom dishes. Following incubation with 500nM of free Ce6 and RGD-HSA-Ce6 with or without free cRGD (10μM), the cells were rinsed with PBS and live cell images were captured with a confocal microscope (Olympus FV1000).

2.4 Intracellular distribution

Live cell confocal microscopy was performed to examine the subcellular distribution of RGD-HSA-Ce6 nanoconjugates. A375 cells were seeded in glass-bottom dishes and transfected with baculovirus expression vectors for GFP chimeras of early endosome (Rab 5), late endosome (Rab 7), lysosome (lysosome-associated membrane glycoprotein 1) and mitochondria (E1 alpha pyruvate dehydrogenase). After attachment, RGD-HSA-Ce6 was added to reach 400nM of Ce6 in the culture medium and the cells were treated for 12h. Then A375 cells were rinsed with PBS and images were captured with a confocal microscope (Olympus FV1000) and merged to determine the intracellular distribution of the nanoconjugates.

2.5 Cytotoxicity of RGD-HSA-Ce6

Dark toxicity. A375 and 3T3 cells (5,000 cells per well in 96-well plates) were incubated with free Ce6 or RGD-HSA-Ce6 (50, 100, 200, 400 and 800nM of Ce6) at 37°C for 48h. After that, cell viability was measured by CCK-8 (Cell

Counting Kit-8) assay. CCK-8 was added into each well and incubated for 2 hours, and then was detected by measuring the absorption at 450nm using a micro plate reader (Safire, TECAN, USA). Cells without any treatment were set as control.

Phototoxicity. A375 and 3T3 cells (5,000 cells per well in 96-well plates) were incubated with free Ce6 or RGD-HSA-Ce6 (50, 100, 200, 400 and 800nM of Ce6) at 37°C for 12h. Then cells were rinsed twice with fresh culture medium and then photo-irradiated with 670nm laser (5mW/cm^2) for 20min. After 24h incubation, cell viability was measured using CCK-8 assay and cells without any treatment were set as control.

Photo-irradiation time dependent Phototoxicity. A375 cells (5,000 cells per well in 96-well plates) were incubated with RGD-HSA-Ce6 (400nM of Ce6) at 37°C for 12h. Then cells were rinsed twice with fresh culture medium and then photo-irradiated with 670nm laser (5mW/cm^2) for 0, 5, 10, 20 and 40min, respectively. After 24h incubation, cell viability was measured using CCK-8 assay. Cells without any treatment were set as control.

2.6 Data analysis

Data are expressed as mean ± SD. Statistical significance was evaluated using t-test for two-sample comparison. * and ** represent $p<0.05$ and $p<0.01$, respectively.

3. Results and discussion

3.1 Preparation of RGD-HSA-Ce6

As shown in Fig.1, Surface amino groups of albumin were reacted with the bifunctional reagent Mal-PEG_{5K}-NHS. After that, the maleimide groups of Mal-PEG_{5K}-NHS were reacted with thiol-containing cyclic RGD peptide. Then activated Ce6 (Ce6-NHS) was conjugated onto the residual amino groups of albumin to form RGD-HSA-Ce6. The concentration of Ce6 (C_{Ce6}) and concentration of HSA (C_{HSA}) of RGD-HSA-Ce6 nanoconjugates were measured at the 403nm absorption peak and BCA assay, respectively. The amount of Ce6 per HSA was obtained from C_{Ce6}/C_{HSA}. The results indicated that about 5.4 Ce6 molecules were conjugated on each HSA.

3.2 Characterization of RGD-HSA-Ce6

The fluorescence of free Ce6 dissolved in PBS/Methanol mixed solvent was much higher than that in PBS, which indicated that most of free Ce6 aggregated in aqueous solution and was dispersed into mixed solvent. In contrast, there was no significant difference between the Ce6 fluorescence of RGD-HSA-Ce6 in PBS or mixed solvent (Sfig. 1). This result indicated that the conjugated Ce6 molecules onto albumin would not be changed by organic solvent. In addition, Fluoraldehyde™ o-Phthaldialdehyde Crystals was used to compare the primary amine of HSA, RGD-PEG-HSA and RGD-HSA-Ce6 with equimolar albumin. Primary amine of unmodified HSA was set as 100%. After modification with PEG and Ce6, primary amine on the surface of albumin gradually decreased to 43.1% and 7.6%, respectively (Sfig. 2).

To investigate the singlet oxygen generation of RGD-HSA-Ce6 in aqueous media, the fluorescence of SOSG before and after photo-irradiation was measured. The singlet oxygen yield of RGD-HSA-Ce6 in aqueous media was approximately 2.3-fold higher than that of free Ce6, which may be attributed to the prevention of Ce6 aggregation in nanoconjugates (Fig. 1b). The average

hydrodynamic diameter and zeta potential of RGD-HSA-Ce6 were 31.1nm and -15.9mV, respectively (Fig. 1c and 1d). Due to the suitable physical properties, RGD-HSA-Ce6 could avoid quick clearance from reticular-endothelial system.[32] TEM image (Sfig. 3) indicated that RGD-HSA-Ce6 was approximately spherical with diameter of about 15-30nm. The slightly smaller size in TEM than DLS was originated from the increase of hydrodynamic volume of nanoconjugates in aqueous condition. The obviously larger diameter of RGD-HSA-Ce6 than unmodified HSA was mainly due to the addition of a PEG coat.[33-35]

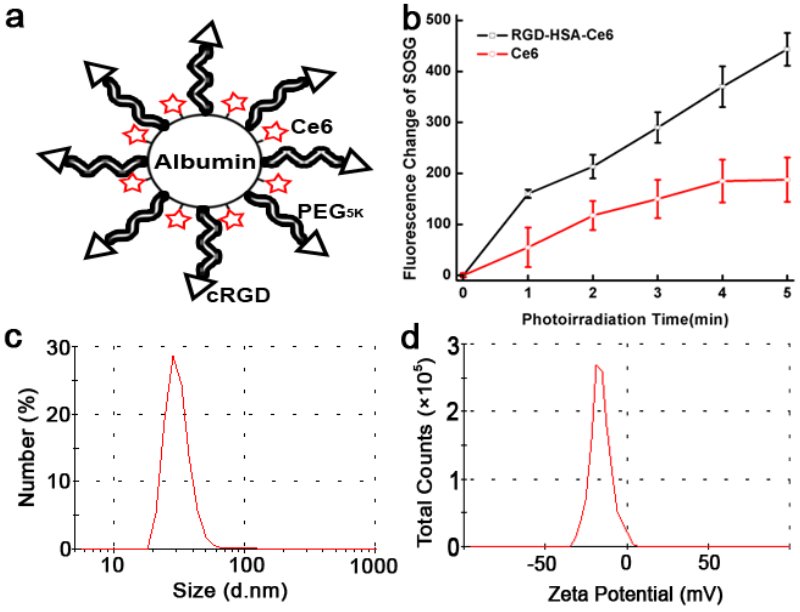

Figure 1: Characterization of targeted nanoconjugates RGD-HSA-Ce6. (a) Schematic graph of RGD-HSA-Ce6. (b) Change of SOSG fluorescence due to singlet oxygen generation by RGD-HSA-Ce6 and free Ce6. Both samples were photo-irradiated for 0, 1, 2, 3, 4 and 5min, respectively (n=3). (c) Particle size distribution and (d) Zeta potential of RGD-HSA-Ce6.

3.3 Intracellular uptake of targeted RGD-HSA-Ce6 nanoconjugates

To compare the tumor-targeting effect of RGD-HSA-Ce6, A375 melanoma cell line with overexpressed αvβ3 integrin was chosen as integrin-positive cell

line.[36, 37] Intracellular uptake of free Ce6 and RGD-HSA-Ce6 was evaluated by incubating with A375 cells for 12h and then detecting by using flow cytometry and confocal microscopy. As shown in Fig. 2, RGD-HSA-Ce6 exhibited significantly higher cellular uptake than free Ce6, suggesting the potential tumor-targeting property of RGD-HSA-Ce6. Receptor blocking experiment was also performed to investigate the uptake profile of RGD-HSA-Ce6. The results indicated that the uptake of RGD-HSA-Ce6 by A375 cells was effectively inhibited when A375 cells were incubated with both RGD-HSA-Ce6 and free cRGD (10μM), a selective inhibitor of integrin αvβ3. This result demonstrated that the selective uptake of RGD-HSA-Ce6 by A375 cells was induced by overexpressed αvβ3 on tumor cells.

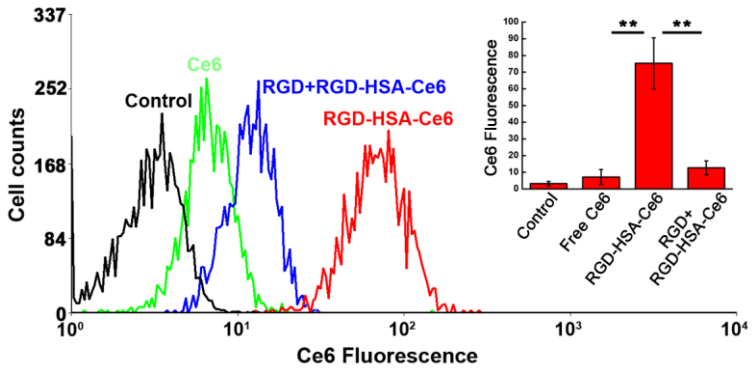

Figure 2: Flow cytometry of intracellular uptake in A375 cells. 200nM of free Ce6 and targeted RGD-HSA-Ce6 nanoconjugates were incubated with A375 cells for 12h and then detected by flow cytometry. 10μM of free RGD was used for selectively blocking αvβ3 integrin. Inset: Quantification of Ce6 fluorescence of each group, data was represented as mean ±SD, n=3, ** p<0.01.

Confocal fluorescent staining was used to further detect intracellular uptake of RGD-HSA-Ce6 by A375 (figure. 3). Ce6 fluorescence (red signal) in A375 cells was observed 12h after incubation with free Ce6 or RGD-HSA-Ce6. It was obvious that the red fluorescence in free Ce6 group was much weaker than that in RGD-HSA-Ce6 group. In addition, the red fluorescent signal of RGD-HSA-Ce6 was dramatically reduced when the integrin αvβ3 is selectively

blocked with the excess cRGD (10μM), which is consistent with the results obtained from flow cytometry.

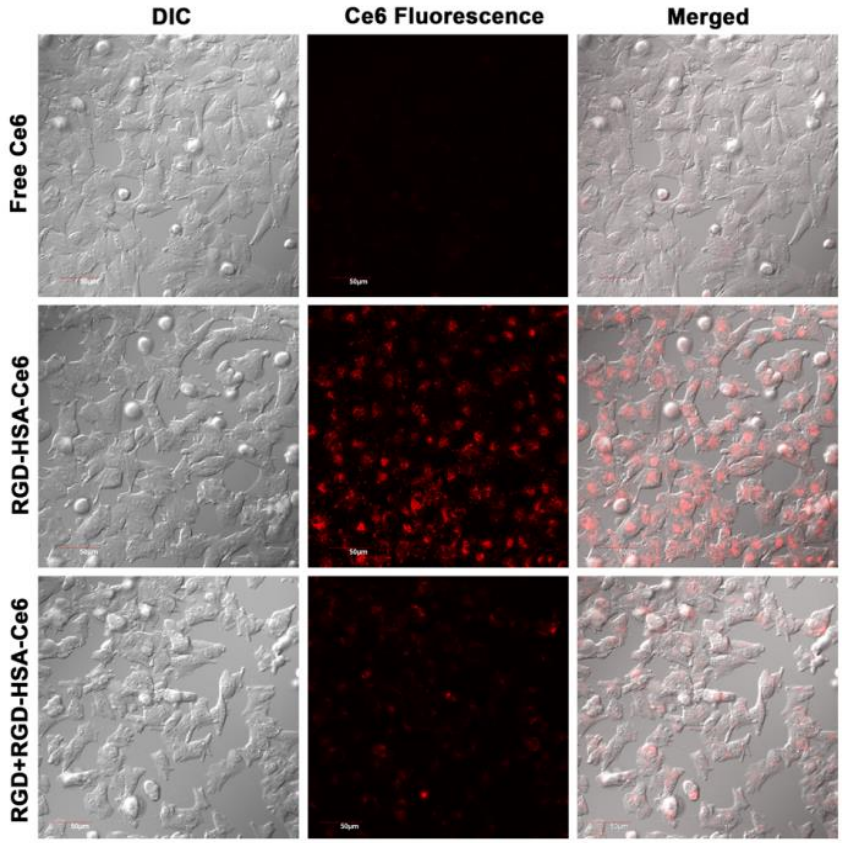

Figure 3: Confocal images of intracellular uptake in A375 cells. Free Ce6 (500nM) and targeted RGD-HSA-Ce6 nanoconjugates (500nM of Ce6) were incubated with A375 cells for 12h. 10μM of free RGD was used for blocking αvβ3 integrin. Scale bar, 50μm.

To further confirm the tumor-targeting property of RGD-HSA-Ce6, uptake of RGD-HSA-Ce6 was also evaluated in a fibroblast cell line (3T3 cells) in which the expression level of integrin αvβ3 was much lower. As shown in Fig. 4, free Ce6 and RGD-HSA-Ce6 showed similar cellular uptake and free cRGD did not showed significant inhibition of the RGD-HSA-Ce6 uptake by 3T3. All these results support the concept that targeted RGD-HSA-Ce6 exhibited enhanced cellular uptake depending on the αvβ3 integrin mediated endocytosis.

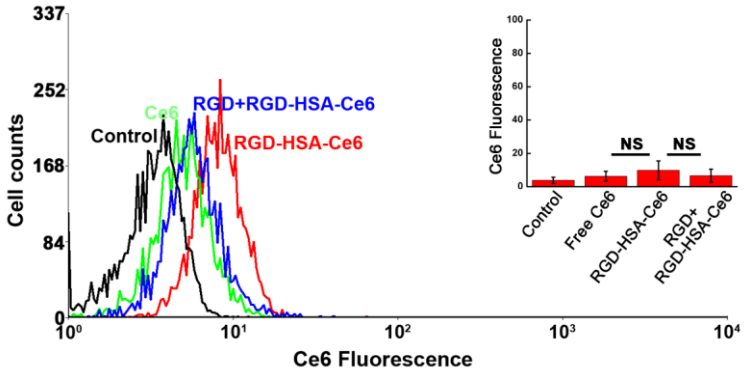

Figure 4: Flow cytometry of intracellular uptake in 3T3 cells. 200nM of free Ce6 and targeted nanoconjugates RGD-HSA-Ce6 were incubated with 3T3 cells for 12h and then detected by flow cytometry. 10μM of free RGD was used for blocking αvβ3 integrin. Inset: Quantification of Ce6 fluorescence of each group, data was represented as mean ±SD, n=3, NS no significance.

3.4 Intracellular distribution of RGD-HSA-Ce6

To further understand the cellular trafficking of the targeted RGD-HSA-Ce6, we utilized chimeras of GFP with marker proteins for specific organelles to visualize the subcellular distribution of RGD-HSA-Ce6 in A375 cells. As seen in Fig. 5, there was considerable co-localization of the fluorescent nanoconjugates with late endosomal and lysosomal GFP markers, indicating that RGD-HSA-Ce6 was mainly transported into late endosomes and lysosomes. In contrast, there was little co-localization of fluorescent RGD-HSA-Ce6 with the early endosomal and mitochondrial GFP marker.

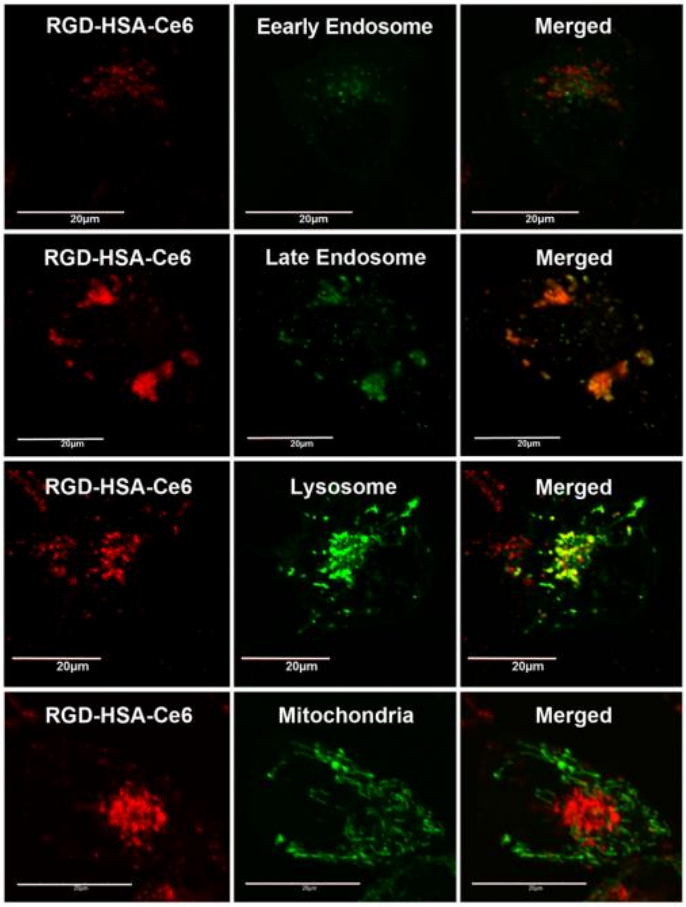

Figure 5: Subcellular localization of RGD-HSA-Ce6. A375 cells were transfected with GFP chimeras that serve as markers for early endosome, late endosome, lysosome and mitochondria. Then cells were incubated with RGD-HSA-Ce6 (400nM of Ce6) for 12h. Live cells were observed by confocal microscopy. Red, Ce6 fluorescence; Green, GFP fluorescence. Scale bar, 20μm.

As shown in Fig.6, the colocalization between RGD-HSA-Ce6 and different organelles was observed by using Pearson's correlation coefficient (PCC). In the late endosome and lysosome groups, the mean PCC value were 0.67 and 0.52, respectively, which were significantly higher than that in early endosome and mitochondria (0.09 and 0.04). These results further confirmed that RGD-HSA-Ce6 was primarily located in late endosomes and lysosomes after endocytosis.

Photo-irradiation of RGD-HSA-Ce6 within tumor cells would generate singlet oxygen that caused oxidative stress to cells. As the half-life and diffusion distance of singlet oxygen were about 0.04μs and 0.02μm, [38, 39] the primary photodynamic damage of RGD-HSA-Ce6 would mainly occur in the late endosomes and lysosomes, in which organelles they were located. Then the photo triggered damage would induce lysosomal membrane permeabilization, release of cathepsins and subsequent cell death.[40]

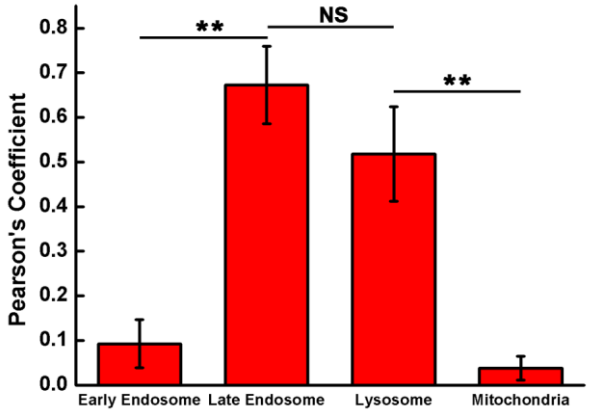

Figure 6: Quantification of Pearson's correlation coefficient between GFP and Ce6 fluorescence. The data was depicted as mean ± SD, n=10, ** p<0.01 and NS no significance.

3.5 Cytotoxicity of RGD-HSA-Ce6 with or without photo-irradiation

To investigate the dark cytotoxicity, free Ce6 and RGD-HSA-Ce6 were added to A375 cells at different concentrations (50 to 800nM of Ce6). Both free Ce6 and RGD-HSA-Ce6 did not exhibit obvious cytotoxicity in dark (Fig. 7a). In order to investigate the laser triggered photocytotoxicity, A375 cells were incubated with free Ce6 and RGD-HSA-Ce6 (50, 100, 200, 400 and 800nM) and photo-irradiated with a 670nm laser (5mW/cm^2) for 20 min. The results indicated that treatment with free Ce6 and photo-irradiation did not exhibit significant cytotoxicity to A375 cells, which was likely due to the poor cellular uptake of free Ce6. However, RGD-HSA-Ce6 exhibited obvious concentration-dependent phototoxicity to A375 cells, which was significantly

higher than free Ce6 (Fig. 7b). In addition, the phototoxicity of RGD-HSA-Ce6 depends on the photo-irradiation time (Fig. 7c).

When compared to free Ce6, RGD-HSA-Ce6 induced more potent PDT to tumor cells, which could be ascribed to higher singlet oxygen generation (Fig. 1b) and enhanced intracellular uptake (Fig. 2). Notably, our results were in contrast with those of Jeong *et al*, which reported that free Ce6 and Ce6-HSA-NPs showed similar phototoxicity to tumor cells.[41] This difference should be attributed to the RGD mediated integrin targeting.

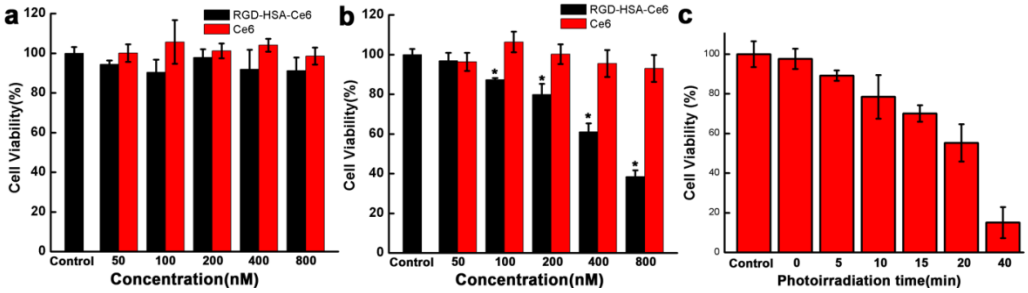

Figure 7: (a) In dark cytotoxicity of free Ce6 and RGD-HSA-Ce6 in A375 cells, n=4. (b) Phototoxicity of free Ce6 and RGD-HSA-Ce6 in A375 cells, n=4. (c) Photo-irradiation time dependent cytotoxicity of RGD-HSA-Ce6 in A375 cells, mean ±SD, n=4, * p<0.05.

Similarly, in dark, free Ce6 and RGD-HSA-Ce6 did not exhibit obvious cytotoxicity to 3T3 cells (Fig. 8a). When the concentration was below 400nM, both free Ce6 and RGD-HSA-Ce6 did not show obvious phototoxicity to 3T3 cells upon photo-irradiation. When the concentration increased to 800nM, RGD-HSA-Ce6 only exhibited slight phototoxicity when compared with free Ce6 (Fig. 8b). These results may be attributed to the low αvβ3 integrin expression on the 3T3 cells and subsequent insufficient cellular uptake of both free Ce6 and RGD-HSA-Ce6.

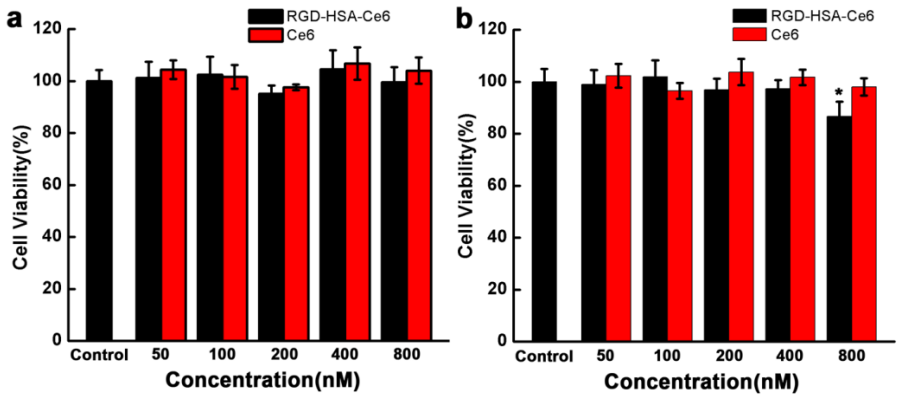

Figure 8: (a) In dark cytotoxicity of free Ce6 and RGD-HSA-Ce6 in 3T3 cells, n=4. (b) Phototoxicity of free Ce6 and RGD-HSA-Ce6 in 3T3 cells, mean ±SD, n=4, * p<0.05.

These results showed that RGD-HSA-Ce6 was highly specific to αvβ3 integrin overexpressing tumor cells, but low phototoxic to normal cells without high αvβ3 integrin expression. During PDT, minimizing normal cells and tissue damage was as important as efficiently killing tumor cells.[42] Therefore, our prepared RGD-HSA-Ce6 might have potential as an in vivo photodynamic therapeutic agent.

4. Conclusion

In summary, we successfully prepared RGD-HSA-Ce6 for tumor targeted photodynamic therapy. RGD-HSA-Ce6 was small size, negative charge and non-toxic in dark. It also exhibited significantly enhanced cellular internalization via αvβ3 integrin mediated endocytosis, and mainly located in late endosomes and lysosomes. Upon photo-irradiation, RGD-HSA-Ce6 produced sufficient singlet oxygen to induce cell death in αvβ3 integrin overexpressed tumor cell line, but not in normal cell line with low αvβ3 integrin overexpression.

Acknowledgments

The authors are grateful to the Program for Changjiang Scholars and Innovative Research Team in University (IRT_14R27) and the National Natural Science Foundation of China (NSFC).

Reference

1. J. Ge, M. Lan, B. Zhou, W. Liu, L. Guo, H. Wang, Q. Jia, G. Niu, X. Huang, H. Zhou, X. Meng, P. Wang, C. S. Lee, W. Zhang and X. Han, *Nat Commun*, 2014, **5**, 4596.
2. L. F. Agnez-Lima, J. T. Melo, A. E. Silva, A. H. Oliveira, A. R. Timoteo, K. M. Lima-Bessa, G. R. Martinez, M. H. Medeiros, P. Di Mascio, R. S. Galhardo and C. F. Menck, *Mutation research*, 2012.
3. M. J. Davies, *Biochemical and biophysical research communications*, 2003, **305**, 761-770.
4. S. P. Glaeser, H. P. Grossart and J. Glaeser, *Environmental microbiology*, 2010, **12**, 3124-3136.
5. M. K. Kuimova, G. Yahioglu and P. R. Ogilby, *Journal of the American Chemical Society*, 2009, **131**, 332-340.
6. A. Gollmer, F. Besostri, T. Breitenbach and P. R. Ogilby, *Free radical research*, 2013, **47**, 718-730.
7. E. O. Serebrovskaya, E. F. Edelweiss, O. A. Stremovskiy, K. A. Lukyanov, D. M. Chudakov and S. M. Deyev, *P Natl Acad Sci USA*, 2009, **106**, 9221-9225.
8. P. Majumdar, R. Nomula and J. Z. Zhao, *J Mater Chem C*, 2014, **2**, 5982-5997.
9. H. Y. Yoon, H. Koo, K. Y. Choi, S. J. Lee, K. Kim, I. C. Kwon, J. F. Leary, K. Park, S. H. Yuk, J. H. Park and K. Choi, *Biomaterials*, 2012, **33**, 3980-3989.
10. H. Park and K. Na, *Biomaterials*, 2013, **34**, 6992-7000.
11. S. Kruspe, C. Meyer and U. Hahn, *Mol Ther-Nucl Acids*, 2014, **3**.
12. X. S. Li, M. R. Ke, M. F. Zhang, Q. Q. Tang, B. Y. Zheng and J. D. Huang, *Chemical communications*, 2015.
13. Y. Li, T. Y. Lin, Y. Luo, Q. Liu, W. Xiao, W. Guo, D. Lac, H. Zhang, C. Feng, S. Wachsmann-Hogiu, J. H. Walton, S. R. Cherry, D. J. Rowland, D. Kukis, C. Pan and K. S. Lam, *Nat Commun*, 2014, **5**, 4712.
14. A. Yuan, J. Wu, C. Song, X. Tang, Q. Qiao, L. Zhao, G. Gong and Y. Hu, *J Pharm Sci*, 2013, **102**, 1626-1635.
15. G. Gong, Q. Pan, K. Wang, R. Wu, Y. Sun and Y. Lu, *Nanotechnology*, 2015, **26**, 045603.
16. G. M. Gong, F. Zhi, K. K. Wang, X. L. Tang, A. Yuan, L. L. Zhao, D. W. Ding and Y. Q. Hu, *Nanotechnology*, 2011, **22**.
17. A. O. Elzoghby, W. M. Samy and N. A. Elgindy, *Journal of controlled release : official journal of the Controlled Release Society*, 2012, **157**, 168-182.
18. Z. Sheng, D. Hu, M. Zheng, P. Zhao, H. Liu, D. Gao, P. Gong, G. Gao, P. Zhang, Y. Ma and L. Cai, *Acs Nano*, 2014, **8**, 12310-12322.
19. Q. Chen, C. Liang, X. Wang, J. He, Y. Li and Z. Liu, *Biomaterials*, 2014, **35**, 9355-9362.
20. H. Jeong, M. Huh, S. J. Lee, H. Koo, I. C. Kwon, S. Y. Jeong and K. Kim, *Theranostics*, 2011, **1**, 230-239.
21. K. Chen and X. Chen, *Theranostics*, 2011, **1**, 189-200.
22. Y. P. Yu, Q. Wang, Y. C. Liu and Y. Xie, *Biomaterials*, 2014, **35**, 1667-1675.
23. H. Yang, C. Y. Qin, C. Yu, Y. Lu, H. W. Zhang, F. F. Xue, D. M. Wu, Z. G. Zhou and S. P. Yang, *Advanced functional materials*, 2014, **24**, 1738-1747.
24. J. D. Humphries, A. Byron and M. J. Humphries, *J Cell Sci*, 2006, **119**, 3901-3903.
25. C. Wang, C. C. Bao, S. J. Liang, H. L. Fu, K. Wang, M. Deng, Q. D. Liao and D. X. Cui, *Nanoscale research letters*, 2014, **9**.
26. J. Kim, H. Y. Nam, J. W. Choi, C. O. Yun and S. W. Kim, *Gene therapy*, 2014, **21**, 476-483.

27. R. Xu, M. Fisher and R. L. Juliano, *Bioconjugate chemistry*, 2011, **22**, 870-878.
28. Z. Cheng, Y. Wu, Z. Xiong, S. S. Gambhir and X. Chen, *Bioconjugate chemistry*, 2005, **16**, 1433-1441.
29. F. Danhier, B. Vroman, N. Lecouturier, N. Crokart, V. Pourcelle, H. Freichels, C. Jerome, J. Marchand-Brynaert, O. Feron and V. Preat, *Journal of controlled release : official journal of the Controlled Release Society*, 2009, **140**, 166-173.
30. X. G. Guan, X. L. Hu, S. Liu, Y. B. Huang, X. B. Jing and Z. G. Xie, *Rsc Adv*, 2014, **4**, 55187-55194.
31. F. F. Wang, L. Chen, R. Zhang, Z. P. Chen and L. Zhu, *Journal of Controlled Release*, 2014, **196**, 222-233.
32. H. Kobayashi, R. Watanabe and P. L. Choyke, *Theranostics*, 2014, **4**, 81-89.
33. A. G. Kanaras, F. S. Kamounah, K. Schaumburg, C. J. Kiely and M. Brust, *Chemical communications*, 2002, 2294-2295.
34. L. J. Cruz, P. J. Tacken, R. Fokkink and C. G. Figdor, *Biomaterials*, 2011, **32**, 6791-6803.
35. J. V. Jokerst, T. Lobovkina, R. N. Zare and S. S. Gambhir, *Nanomedicine*, 2011, **6**, 715-728.
36. H. Q. Yin, F. L. Bi and F. Gan, *Bioconjugate chemistry*, 2015, **26**, 243-249.
37. H. Q. Yin, D. S. Mai, F. Gan and X. J. Chen, *Rsc Adv*, 2014, **4**, 9078-9085.
38. S. G. Awuah and Y. You, *Rsc Adv*, 2012, **2**, 11169-11183.
39. J. Shao, Y. Dai, W. Zhao, J. Xie, J. Xue, J. Ye and L. Jia, *Cancer letters*, 2013, **330**, 49-56.
40. P. Boya and G. Kroemer, *Oncogene*, 2008, **27**, 6434-6451.
41. H. Jeong, M. Huh, S. J. Lee, H. Koo, I. C. Kwon, S. Y. Jeong and K. Kim, *Theranostics*, 2011, **1**, 230-239.
42. A. A. Rosenkranz, D. A. Jans and A. S. Sobolev, *Immunology and cell biology*, 2000, **78**, 452-464.